Journal of Solution Chemistry, Vol. 21, No. 8, 1992

Measurement of pH in Subcritical and Supercritical Aqueous Systems[1]

Digby D. Macdonald,[2,3] Samson Hettiarachchi,[4] Herking Song,[5] Kari Makela,[6] Rob Emerson,[4] and Mordehai Ben-Haim[7]

Received September 16, 1991; Revised February 26, 1992

The use of yttria-stabilized zirconia (YSZ) electrodes of the type $Hg/HgO/ZrO_2(Y_2O_3)/H^+$, for measuring pH in aqueous solutions at high subcritical ($150 < T < 374°C$) and supercritical temperatures ($T > 374°C$) is reviewed. The construction and operation of the YSZ and reference electrodes employed in these studies are described and their application in measuring the pH of a variety of technologically-important aqueous system is discussed. We show that the YSZ electrode is thermodynamically viable at temperatures into the supercritical region, and that it is a primary pH sensor in that calibration is not necessary, provided that the activity of water is known. However, highly accurate pH measurements at high subcritical and supercritical temperatures will require the development of more accurate reference electrodes.

KEY WORDS: pH measurements; supercritical solutions; subcritical solutions; reference electrodes

[1]Presented at the Second International Symposium on Chemistry in High Temperature Water, Provo, UT, August 1991.

[2]Center for Advanced Materials, The Pennsylvania State University, University Park, PA 16802.

[3]To whom correspondence should be addressed.

[4]SRI International, Menlo Park, CA 94025.

[5]VTT, Espoo, Finland.

[6]Molecular Devices, Menlo Park, CA 94025.

[7]Nuclear Research Center, Negev, Beer Sheva, Israel.

0095-9782/92/0800-0849$06.50/0

1. Introduction

The activity of hydrogen ion a_{H^+} is a key parameter in describing the thermodynamic and kinetic properties of processes occurring in aqueous solutions. Because of the wide range over which a_{H^+} may vary (practically from >1 to $<10^{-14}$ at 25°C), due to the magnitude of the dissociation product of water ($K_w = 10^{-14}$ at 25°C), it is common practice[1] to express a_{H^+} on a logarithmic scale as pH

$$pH_T = -\log(a_{H^+}) = -\log(m_{H^+}\gamma_{H^+}) \quad (1)$$

where m_{H^+} and γ_{H^+} are the molal concentration and activity coefficient of an hydrogen ion, respectively, in the system.

The quantity defined by Eq. (1) may be termed the "thermodynamic pH," because it is expressed in terms of the hydrogen ion activity. However, it contains a quantity γ_{H^+} that is not experimentally accessible. For this reason, other definitions have been employed,[1,2] including those related to various concentration scales (as opposed to activity)

$$pH_m = -\log(m_{H^+}) \quad (2)$$

$$pH_M = -\log(M_{H^+}) \quad (3)$$

where M_{H^+} is the molar hydrogen ion concentration. As pointed out by Mesmer,[2] the definition afforded by Eq. (2) [and hence also by Eq. (3)] offers the significant advantage that the pH can be expressed as

$$pH_m = -\log(a_{H^+}a_{Cl^-}) + \log m_{Cl^-} + \log(\gamma^2_{\pm,HCl}) \quad (4)$$

in that all of the quantities on the right hand side are known (m_{Cl^-}) or can be measured ($a_{H^+}a_{Cl^-}$, $\gamma_{\pm,HCl}$) directly. Thus, $a_{H^+}a_{Cl^-}$ can be measured using the Harned cell without liquid junction and $\gamma_{\pm,HCl}$ is also often known from direct measurements.

Notwithstanding the confusion that sometimes results because of the existence of multiple definitions of 'pH,' the choice of any particular definition is normally made for operational convenience, either because a particular pH sensor is calibrated against standard buffers or because a particular electrochemical cell is employed in the measurements. In the present work, we define pH in the thermodynamic sense [Eq. (1)], principally because the pH sensor employed in the majority of our studies (the yttria-stabilized zirconia electrode) senses hydrogen ion activity. This definition has the distinct advantage that it is directly related to a well-defined thermodynamic scale [the Standard Hydrogen Electrode (SHE) scale], but it has the disadvantages that the pH can only be related to the other definitions by knowing the activity coefficient for H^+,

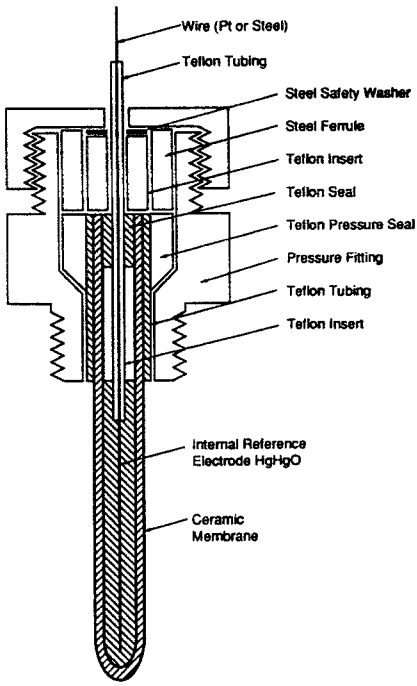

Fig. 1. Typical Yttria-stabilized zirconia pH sensor.

(which is not accessible experimentally) and that the isothermal liquid junction potential must be estimated.

It is not our intention, in this paper, to review the many techniques for measuring pH. Instead, we restrict our discussion to one specific electrode [the yttria-stabilized zirconia (YSZ) membrane electrode] for measuring pH in aqueous systems at elevated temperatures,[3] and we review recent efforts in our laboratory to extend pH measurements to supercritical temperatures. To our knowledge, the work reported here represents the first attempt to measure pH at temperatures above the critical temperature of water.

2. Experimental Techniques

2.1. The Yttria-Stabilized Zirconia Electrode

The yttria-stabilized zirconia (YSZ) sensor was originally described by Niedrach in 1980 as a reference electrode and pH sensor, and was subsequently used extensively to measure the pH of aqueous solutions at subcritical temperatures up to 300°C by Macdonald and

coworkers[3,5-7] and others[8]. This electrode has proven to be rugged and serviceable, and is currently well-suited for physico-chemical investigations in high temperature aqueous systems, when high accuracy is not required. The current restriction on accuracy, however, is not an inherent limitation of the YSZ sensor but arises because of the current lack of a correspondingly accurate reference electrode, as discussed later in this paper.

Typically, a YSZ pH sensor consists of an oxygen ion-conducting ZrO_2 (9% Y_2O_3) ceramic tube containing a metal/metal oxide reference element (Fig. 1). Accordingly, the sensor may be represented in the formal sense as

$$\begin{matrix} M/M_xO_y \mid ZrO_2(Y_2O_3) \mid H^+, H_2O \\ \phi_{r,r} \quad I \; \phi_{z,r} \qquad \phi_{z,s} \; II \; \phi_{ss} \end{matrix} \tag{5}$$

where ϕ is the electrical potential and subscripts (r,r), (z,r), (z,s), and (s,s) denote the reference side of the reference interface (I), the ceramic side of the reference interface, the ceramic side of the YSZ/solution interface (II), and the solution side of that interface, respectively. Because YSZ is exclusively an oxygen ion conductor, the reactions that occur at interfaces I and II can be written as

$$(1/y)M_xO_y + V_O^{\cdot\cdot} + 2e' \rightleftharpoons O_O + (x/y)M \tag{6}$$

$$V_O^{\cdot\cdot} + H_2O \rightleftharpoons O_O + 2H^+ \tag{7}$$

respectively, where $V_O^{\cdot\cdot}$ designates (in Kroger-Vink notation) an oxygen vacancy in the YSZ lattice (with double positive charge) and O_O signifies an oxide ion in a normal anion site in the lattice. At equilibrium, the sum of electrochemical potentials

$$\tilde{\mu} = \mu_i^o + RT\ln a_i + z_iF\phi \tag{8}$$

for species on each side of reactions (6, 7) must be equal, where μ_i^o is the standard chemical potential, a_i is the activity of the i^{th} species (of charge z_i), and ϕ is the electrical potential in the various phases as shown in Cell (5). Equilibrium at the two interfaces therefore stipulates that

$$\phi_{r,r} - \phi_{z,r} = -\Delta\mu_1^o/2F + (RT/2F)\ln(a_{V_O^{\cdot\cdot},r}) \tag{9}$$

$$\phi_{z,s} - \phi_{s,s} = -\Delta\mu_2^\circ/2F - (RT/2F)\ln(a_{V_O^{\cdot\cdot},s}) - (RT/2F)\ln(a_{H_2O}) - (2.303RT/F)\text{pH} \quad (10)$$

where $\Delta\mu^\circ$ is the change in standard chemical potential; $(a_{V_O^{\cdot\cdot},r})$ and $(a_{V_O^{\cdot\cdot},s})$ are the activities of oxygen vacancies $V_O^{\cdot\cdot}$ in the YSZ membrane at the reference (M/M_xO_y) and solution sides, respectively, and a_{H_2O} is the activity of water. Subscripts r and s are defined as referring to the reference side and the solution side, respectively, of the membrane with the additional definitions given above. Subtraction of Eq. (10) from Eq. (9) yields the potential of the YSZ sensor on the standard hydrogen electrode (SHE) scale as

$$E = E^\circ_{M_xO_y} - \left(\frac{RT}{2F}\right)\ln(a_{H_2O}) - \left(\frac{2.303RT}{F}\right)\text{pH} \quad (11)$$

where the standard potential $E^\circ_{M_xO_y}$ is related to the change in standard chemical potential $\Delta\mu_R^\circ$ for the reaction

$$(1/y)M_xO_y + H_2 \rightleftarrows (x/y)M + H_2O \quad (12)$$

by

$$E^\circ_{M_xO_y} = -\Delta\mu_R^\circ/2F \quad (13)$$

The analysis described above leads to a number of very important consequences for the performance of the YSZ pH sensor:

1. The equilibrium potential is independent of the properties of the ceramic membrane, provided that the measurement is made potentiometrically ($\phi_{z,r} = \phi_{z,s}$) and the ceramic is of uniform composition and defect structure ($a_{V_O^{\cdot\cdot},r} = a_{V_O^{\cdot\cdot},s}$).

2. For a given water activity and pH, the equilibrium potential depends only on the standard potential of the internal reference couple. Consequently, the YSZ sensor is a primary pH electrode (*i.e.*, it does not need calibrating). Furthermore, the best internal reference has a stoichiometric composition, a single oxidation state, and accurately known thermodynamic properties. Of all the metal/metal oxide couples available, Hg/HgO appears to fulfill these requirements most completely. Other couples that have been

employed (*e.g.*, Cu/Cu_2O_4 or oxygen gas[8]) are not suitable for highly accurate work, because one or more of the conditions stated above are not met with sufficient precision. However, because of the toxicity of mercury, other couples may be desirable for many applications at the expense of accuracy. In this regard, we have found that Ag/Ag_2O and Ni/NiO are both quite acceptable as internal reference elements. Although the thermodynamic stability of Ag_2O above 150°C is questionable, our data showed that Ag_2O is kinetically stable even at 275°C for short periods of time. The lack of stoichiometry in NiO is a matter of concern for accurate laboratory work, but the Ni/NiO couple does appear to be suitable for the purposes of pH monitoring in industrial environments.

3. Because $ZrO_2(Y_2O_3)$ is a wide band-gap material, electronic conductivity is negligible so that the YSZ sensor does not respond to changes in the redox potential of the system. This is a most important property of the YSZ electrode, because the redox potential may be adjusted to stabilize a species of interest in the solution. For example, the YSZ sensor could be used to study the hydrolysis of Cu^{2+} by stabilizing Cu(II) with oxygen, whereas the same measurements are not feasible using a hydrogen electrode.

The advantages outlined above are partially offset by the need to know the activity of water. For dilute solutions, the error incurred in ignoring the water activity term (*i.e.*, by assuming $a_{H_2O} = 1$) is negligible for all but the most accurate work, but at high ionic strengths the contribution of this term to the pH can be substantial. We have found that, for most applications, the activity of water may be estimated from osmotic coefficient data for NaCl solutions (Liu and Lindsay[9]) at equivalent ionic strengths. We caution, however, that this must be regarded as a first approximation only, and that highly accurate work may require the simultaneous measurement of the activity of water by independent means (*e.g.*, by measuring the vapor pressure). Another problem experienced when using the YSZ sensor arises from the high electrical resistance of the ceramic membrane, particularly at lower temperatures. Typically, the resistivity of the membrane changes from 10^7 - 10^8 Ω-cm

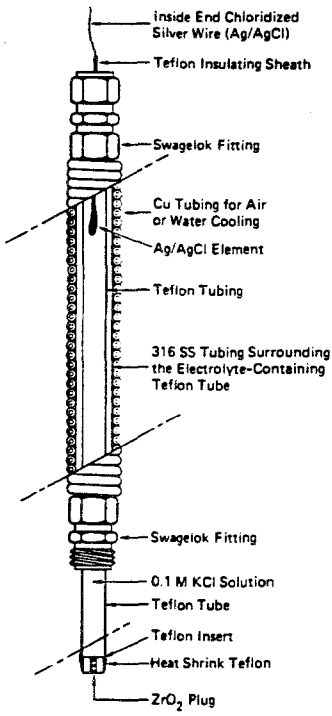

Fig. 2. External pressure-balanced reference electrode assembly.

at 100°C to $< 10^5$ Ω-cm at 300°C. The resistivity at the lower temperature is sufficiently high to give rise to considerable electrical problems in measuring the cell voltage due to stray current leakage around insulated fittings. Practically, we have found that the lower temperature limit for reliable pH measurements is about 125°C.

2.2. Reference Electrodes

In determining the pH of a solution, the parameter that is actually measured experimentally is the voltage of the YSZ sensor against a suitable reference electrode. Before describing the types of reference electrodes that have been used in high temperature aqueous solution studies, it is first necessary to identify those characteristics that are desired in reference electrodes for reliable pH measurements,[10] particularly at elevated temperatures ($T > 100$°C). The desired properties are as follows:

1. The electrode needs to be sufficiently rugged to withstand the high temperatures and pressures inherent in these

studies and to survive the large changes in temperature and pressure associated with heat-up and cool-down of the apparatus.

2. The electroactive element of the reference electrode must be thermally and chemically stable at the prevailing temperatures, and must not exhibit a mixed potential associated with non-conjugate anodic and cathodic reactions.

3. The internal solution in contact with the electroactive element should be well-defined thermodynamically, in that the activity of the potential-determining ion must be known at the temperature, pressure, and concentration of interest.

4. The transport properties and concentration of the internal solution should be such that the liquid junction potential between the internal and external environments is reduced to as low a value as possible or can be estimated reliably.

5. A most important characteristic of any reference electrode is that its potential must be related to a rational thermodynamic scale (*e.g.*, the SHE scale), either by calculation or by direct calibration. Care must be taken to ensure that, in the first case, the electrode operates in the true equilibrium state and, in the second, the reference electrode potential is reproducible and reversible and does not exhibit significant hysteresis over the entire range of conditions (T, P, composition) of operation.

Broadly speaking, the reference electrodes that have been used in high temperature aqueous studies can be divided into two classes: (i) external reference electrodes of which the External Pressure Balanced Reference Electrode (EPBRE) is the most prominent member, and (ii) internal reference electrodes (IREs). It is not our intention to review reference electrode technology in detail, because this has been done elsewhere.[10-12] Instead, we will concentrate on EPBREs, which have been used extensively at high subcritical temperatures,[12] and on two novel IREs, both of which show promise for extending pH measurements above the critical temperature of water (374°C).

(i) External Pressure Balanced Reference Electrodes. The EPBRE was introduced by Macdonald, Scott, and Wentrcek[12] in 1981 in an attempt to produce a highly stable reference electrode for monitoring potentials in high temperature aqueous systems over extended periods of time. The principal problem that this design attempted to address was the thermal hydrolysis of the electroactive element (*e.g.*, AgCl $\rightarrow$ Ag_2O $\rightarrow$ Ag) that has plagued aqueous electrolyte internal reference electrodes when operated for long times at high temperatures, particularly under reducing conditions.[11] The EPBRE (Fig. 2) addresses this problem by maintaining the electroactive Ag/AgCl element at ambient temperature, at the expense of forming a thermal liquid junction potential along the non-isothermal electrolyte column contained in the deformable PTFE inner compartment. A deformable compartment was employed so that volume changes on pressurization could be accommodated without significant flow through the porous zirconia, isothermal liquid junction. Furthermore, deformation of the PTFE compartment transmits pressure pulses into the internal solution, thereby preventing thermal diffusion and hence the establishment of a Soret steady state. Accordingly, the EPBRE is designed to operate in the Soret initial state, and the thermal liquid junction potentials derived from calibrating the electrode refer to this condition. It is important to note that the EPBRE is strictly a non-equilibrium electrode because of thermal diffusion. In principal, the potential of the EPBRE can be calculated by knowing the entropies of transport of K^+ and Cl^- and the thermodynamics of KCl solution at the cold end of the junction. In practice, however, it is much more convenient to calibrate the electrode against an Ag/AgCl, internal reference electrode in a solution of the same KCl concentration as the EPBRE internal solution (0.1 m), so that the isothermal liquid junction potential is zero. Typical calibration data are shown in Fig. 3 and have been expressed in polynomial form as

$$E_{SHE}(T) = E_{obs} + 0.286637 - 1.003217\times10^{-3}\Delta T + 0.0174478\times10^{-5}\Delta T^2 - 0.3030048\times10^{-8}\Delta T^3 \quad (14)$$

where $E_{SHE}(T)$ is the potential of the indicator electrode on the SHE scale at temperature T, E_{obs} is the observed potential with respect to the EPBRE, and $\Delta T = T - 298.15K$. A somewhat more accurate correlation, extending to temperatures as high as 400°C, was recently determined in our laboratory as

$$E_{SHE}(T) = E_{obs} + 2.8159\times10^{-3} + 4.2802\times10^{-4}\Delta T - 2.8170\times10^{-7}\Delta T^2$$

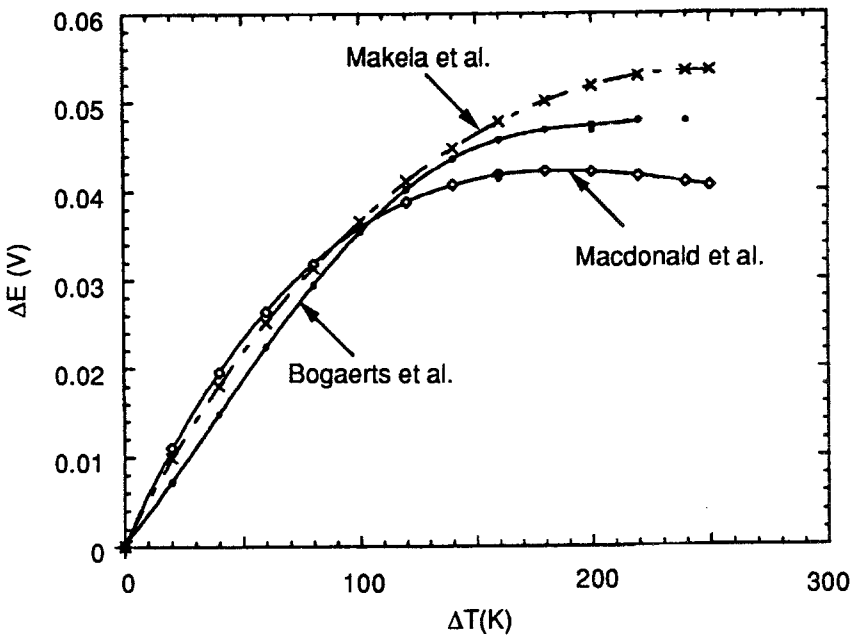

Fig. 3. Thermocell potentials for the cell (298.15 K) Ag-AgCl/KCl/KCl(0.1*m*)/AgCl-Ag [*T* (K) as a function of $\Delta T(= T - 298.15)$].

$$- 1.2650\times10^{-8}\Delta T^3 + 7.4738\times10^{-11}\Delta T^4 \qquad (15)$$

which is in good agreement with that of Bogaerts[14] for temperatures from 25 to 300°C (the extent of his calibration). Thermal liquid junction potentials (TLJPs) for alkali halide solutions have been calculated from data of the type summarized above and some of the TLJP data are plotted in Fig. 4. The thermal liquid junction potential is found not to be a strong function of concentration and to be nearly independent of the identity of the cation. Finally, the thermal liquid junction potential data could be accounted for quite well by a simple ion in a uniform dielectric medium model, indicating that the principal contribution to the potential is electrostatic in nature.[15]

The isothermal liquid junction potential (ILJP) that is established by ionic diffusion across the porous zirconia plug (Fig. 2) must be corrected if accurate pH values are to be derived. In principle, the ILJP can be calculated using the following equation

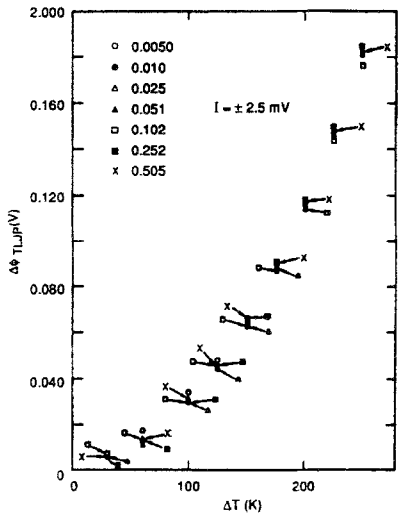

Fig. 4. Thermal liquid junction potentials as a function of $\Delta T(= T - 298.15K)$ for various KCl concentrations (M).

Table I. Calculated Isothermal Liquid Junction Potentials for the Junction 0.1m KCl/1m NaOH

T(°C)	$E_j^{Henderson\,a}$	$E_j^{Corr\,b}$	$E_j^{T\,c}$	$E_j^{Mesmer\,d}$
25	47.0	-3.0	44.0	29.6
50	49.2	-3.3	45.9	31.1
100	48.0	-3.6	44.4	31.0
150	45.1	-3.9	41.2	29.7
200	42.3	-4.2	38.0	28.2
250	40.0	-4.8	35.2	27.0
300	38.7	-5.9	32.9	26.3

[a] Equation (17). [b] Activity coefficient correction. [c] Equation (16) assuming concentration-independent transport numbers. [d] Ref. 2 mean concentration approximation.

$$E_j = -\frac{RT}{F}\sum_i \int_{(1)}^{(2)} (t_i/z_i) d\ln a_i \qquad (16)$$

where t_i is the transport number for the i^{th} ion (charge z_i), a_i is the ion activity ($a_i = m_i\gamma_i$), and the integral is evaluated across the junction from phase (1) to phase (2). By ignoring activity coefficient effects, Eq. (16) reduces to the Henderson[16] equation

$$E_j = -\frac{RT}{F}\frac{W_2 - W_1}{U_2 - U_1}\ln\left(\frac{U_2}{U_1}\right) \tag{17}$$

where $$U = \sum_j \lambda_j |z_j| m_j, \quad w = \sum_i \lambda_i |z_i| m_i / z_i$$

and the subscripts 1 and 2 designate the boundaries of the junction. Because activity coefficient effects are ignored, Eq. (17) provides only a rough approximation of the actual liquid junction potential, which becomes less reliable as the ionic strength increases. An even more approximate form of Eq. (16) is commonly used[2,17] and is obtained by writing $d\ln(m_i) \sim dm_i/\bar{m}_i$ where $\bar{m}_i$ is the average concentration of species i across the junction. However, this approximation breaks down badly when the liquid junction potential exceeds a few tenths of a millivolt, and it is not recommended unless conditions are chosen that this constraint is fulfilled (*e.g.*, by using very high KCl concentrations in the electrode). The importance of activity coefficient effects and the viabilities of various approximations to Eq. (16) have been recently explored by Pang and Macdonald[18] and will be published shortly. The importance of using the full form of Eq. (16) for estimating ILJPs is illustrated in Table I for the junction 0.1*m* KCl|1*m* NaOH at temperatures ranging from 25 to 300°C. Thus, the activity coefficient correction (for this particular case) is 7-12% of the ILJP calculated using the Henderson equation, and the potential, calculated using Mesmer's approximation,[2] are more than 25% lower than the value estimated using Eq. (16) over the entire temperature range. It should be noted that even the latter value is an approximation because the concentration dependencies of the transport numbers have been ignored. Given the difficulties inherent in estimating ILJPs it is recommended that the conventional approach of suppressing liquid junction potentials using a suitably high KCl concentration on the left side of the junction be employed if at all possible. However, the viability of this approach depends heavily on the composition of the solution on the right side of the junction and for highly concentrated solutions suppression may not be possible.

Compared with an Ag/AgCl, (KCl solution) IRE of the type originally used by Greeley *et al.*,[19] the EPBRE is less accurate due to the uncertainty in the TLJP. However, EPBREs offer considerable advantages in terms of long term stability and serviceability, and they are ideally suited for measuring potentials in systems where moderate accuracy is acceptable (*e.g.*, in corrosion and solubility studies). For highly accurate pH studies, internal reference electrodes are still

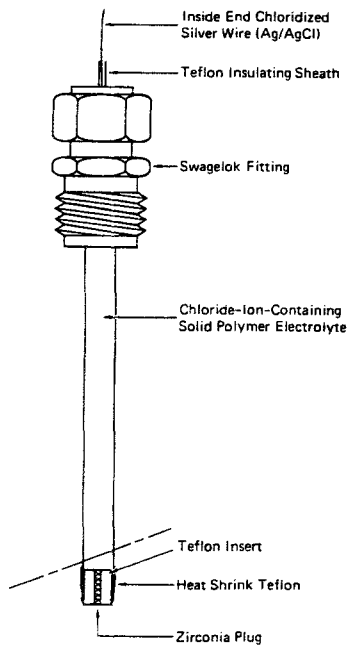

Fig. 5. Solid polymer electrolyte based internal reference electrode.

preferred, but they must be handled with care to avoid potential drift due to the thermal hydrolysis of the reference element.

(ii) Internal Reference Electrodes. The general design and operation of IREs has been discussed at length elsewhere,[11,20] so that the present discussion is restricted to two recent innovations that were made to extend the temperature of operation above 300°C and ultimately into the supercritical region ($T > 374°C$). The principal drawback of IREs based on the Ag/AgCl, (KCl soln.) electroactive element is thermal hydrolysis of AgCl, which generates a mixed potential rather than an equilibrium potential as well as changing the chloride activity. Nevertheless, the Ag/AgCl element is one of the most accurate and serviceable in electrochemistry, so that considerable incentive exists for retaining its use in the study of high temperature aqueous systems. In an attempt to increase the temperature range over which this reference system may be used, we recently devised a polymer electrolyte reference electrode consisting of a KCl electrolyte dispersed in an epoxy matrix (Fig. 5). The electrolyte sets as a rubber, with the result that the electrode within the pressure vessel is easily manipulated to produce the optimum configuration. The performance of this electrode is shown in Fig. 6. Because the thermodynamic properties of KCl in the electrolyte

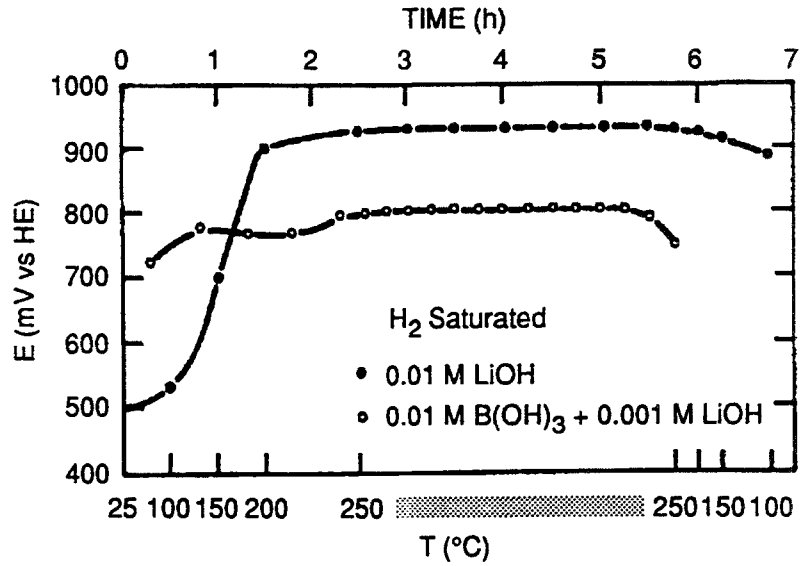

Fig. 6. Performance of the polymer internal reference electrode as function of temperature. The potential of the electrode was measured against that of a hydrogen electrode in the same solution saturated with hydrogen at ambient temperature.

are ill-defined, it is not possible to calculate the potential *a priori* from theory. Nevertheless, the electrode is readily calibrated and has provided stable performance over many hours at temperatures as high as 275°C. In one instance, polymer electrolyte reference electrode was inadvertently taken to ~340°C for a short time with no apparent ill-effects.

In the second case, we devised a Ag/AgCl electrode with a soda glass (KCl) electrolyte. While this electrode exhibits extraordinarily high impedances at low temperatures, the impedance of the electrolyte is sufficiently low at temperatures above 300°C that it can be used for potential measurements. However, as with the polymer electrolyte electrode, the glass electrolyte reference electrode must be calibrated to the SHE scale because the thermodynamic properties of KCl in glass are unknown.

3. Thermodynamic Viability

Although we have previously published[3] our findings on the thermodynamic viability of the YSZ electrode, it is worth repeating some of the details here because they indicate the level of precision that

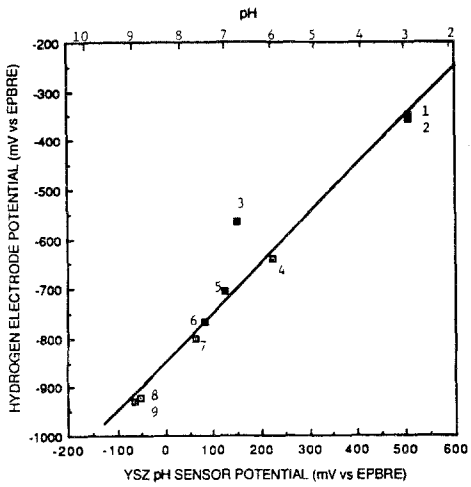

Fig. 7. Plot of the hydrogen electrode potential against the YSZ electrode potential at 200°C for standard solutions. 1, 0.1*m* $NaHSO_4$; 2, 0.01*m* H_3PO_4; 3, 0.01*m* $B(OH)_3$; 4, 0.1*m* H_3PO_4 + 0.14*m* NaOH; 5, 0.01*m* $B(OH)_3$ + 0.0001*m* KOH; 6, 1*m* Na_2SO_4; 7, 0.01*m* $B(OH)_3$ + 0.001*m* KOH; 8, 0.01*m* $B(OH)_3$ + 0.01*m* KOH; and 9, 0.01*m* KOH.

the YSZ electrode is capable of when measuring pH. The most effective way of assessing the thermodynamic viability is to measure the potential of the YSZ electrode against an electrode whose pH response is known (or assumed *a priori*) to be Nernstian. The most suitable electrode for this purpose is the hydrogen electrode, and plots of this type for temperatures of 200 and 300°C are shown in Figs. 7 and 8. Each point in these plots refers to a different solution, which were chosen to span the high temperature pH range from about 3 to 9, as indicated by the upper scale. The pH values listed on the upper ordinate were calculated from the potential of the hydrogen electrode measured against an EPBRE on the SHE scale.

From Eq. (11) and the Nernst equation for the H_2/H^+ system, we may express the potential of the hydrogen electrode E_H as a function of that for the YSZ electrode E_{YSZ}, both measured against a common reference electrode, as

$$E_H = E_{YSZ} - E^\circ_{Hg/HgO} - \frac{2.303RT}{2F}[\log f_{H_2} - \log a_{H_2O}] \qquad (18)$$

Because the solutions employed in this analysis are relatively dilute, $a_{H_2O} \sim 1$, and since the fugacity of hydrogen was established under am-

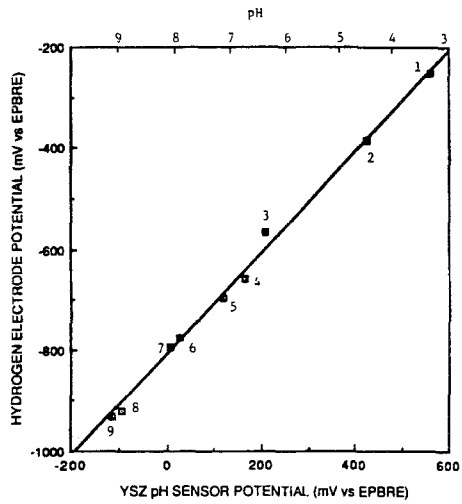

Fig. 8. Plot of the hydrogen electrode potential against the YSZ electrode potential at 300°C for standard solutions. 1, 0.01*m* H_3PO_4; 2, 0.01*m* $NaHSO_4PO_4$; 3, 0.01*m* $B(OH)_3$; 4, 0.1*m* H_3PO_4 + 0.14*m* NaOH; 5, 00.01*m* $B(OH)_3$ + 0.0001*m* KOH; 6, 1*m* Na_2SO_4; 7, 0.01*m* $B(OH)_3$ + 0.001*m* KOH; 8, 0.01*m* $B(OH)_3$ + 0.01*m* KOH; and 9, 0.01*m* KOH.

bient conditions by sparging the reservoir, f_{H_2} is constant (ignoring small salting-in/salting-out corrections). Accordingly, the last term on the right hand side of Eq. (18) is constant (as is $E^{\circ}_{Hg/HgO}$ for any given temperature), so that a plot of E_H *vs.* E_{YSZ} should be linear, as observed, only if the YSZ electrode exhibits a Nernstian dependence on pH. Furthermore, the intercept at $E_{YSZ} = 0$ is found to be in accord (to within ±5 mV) with the known standard potential of the Hg/HgO couple. Interestingly, the point for 0.01*m* $B(OH)_3$ was found to lie to the left of the correlation by an amount that decreases rapidly with increasing temperature. The fact that the problem lies with the YSZ electrode is clearly evident by noting that the pH of 0.01 m $B(OH)_3$ at 200°C is 5.4, as determined by calculation and measurement using a hydrogen electrode against a suitably calibrated reference. This anomalous behavior disappears when a small amount of LiOH is added to the solution, as shown in Fig. 7.

A second feature of the data plotted in Figs. 7 and 8 is that they indicate the level of precision that may be achieved in the measurement of pH using a YSZ electrode in the absence of errors in a reference electrode. Close examination of these data indicates that the YSZ electrode is precise [*i.e.*, conforms to Eq. (11)] to better than ±10 mV at

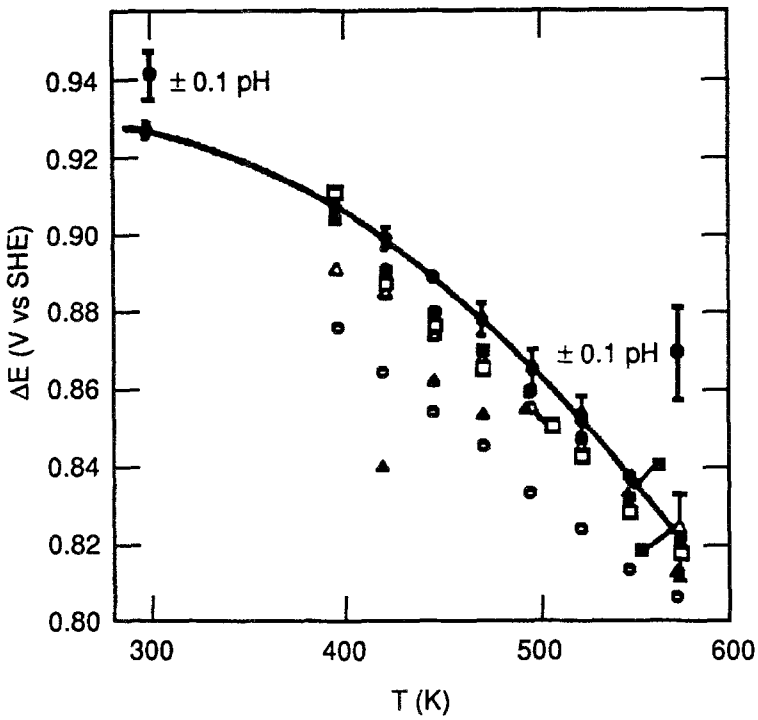

Fig. 9. Plot of ΔE *vs.* temperature for the cellH_2, H_2O/YSZ/HgO/Hg. ▲, 0.01*m* H_3PO_4; o, 1*m* Na_2SO_4; Δ, 0.01 *m* $(B(OH)_3 + 0.01m$ KOH; □, 0.01*m* KOH; ■, extrapolated to zero ionic strength; and •, theory.

200°C and to better than ±5 mV at 300°C, with much of these differences being traceable to variations in the last term in Eq. (18) from solution to solution. Accordingly, when using a precisely calibrated reference electrode, the YSZ sensor should be capable of yielding pH values to better than ±0.05 units. This level of precision renders the YSZ electrode quite suitable for precise thermodynamic and solution chemistry measurements.

Another way of displaying and assessing the thermodynamic viability of the YSZ electrode is to replot (Fig. 9) the data as a function of temperature as

$$\Delta E = E^{\circ}_{Hg/HgO} + \frac{2.303RT}{2F} \log\left[\left(\frac{K^{\circ}_H}{K^{T}_H}\right)\left(\frac{\gamma^{T}_{H_2}}{\gamma^{\circ}_{H_2}}\right)\left(\frac{f^{\circ}_{H_2}}{a^{T}_{H_2}}\right)\right] \tag{19}$$

where K_H is Henry's constant for hydrogen in water, γ_{H_2} is the activity coefficient for hydrogen, f_{H_2} is the fugacity, and a_{H_2O} is the activity of

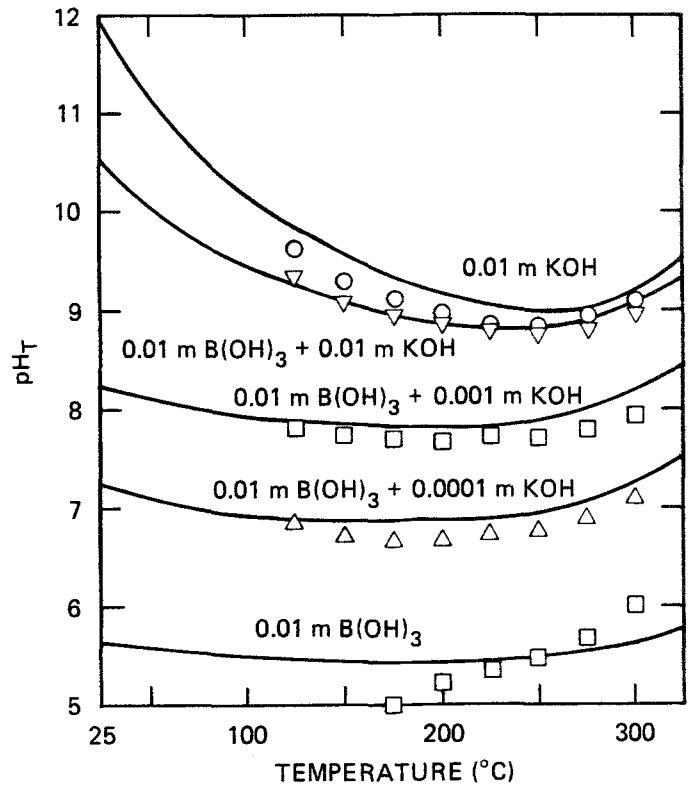

Fig. 10. pH *vs.* temperature correlations for various $B(OH)_3$/KOH solutions. Discrete points ≡ experimental data and solid lines ≡ MULTEQ calculations.

water. The superscripts "o" and "T" designate the reference temperature of 25°C and test temperature, respectively. In deriving Eq. (19), we have included corrections for the activity of water and for the salting-in/salting-out of hydrogen, as described elsewhere.[3] For example, water activities were calculated from the extensive data of Liu and Lindsay[9] for NaCl solutions using the "equivalent ionic strength" approximation. Salting-in/salting-out was corrected using the Sechenov coefficients listed by Naumov *et al.*[21] As can be seen from Fig. 9, data for the solutions agree quite well with the theoretical behavior (to within ±0.1 pH unit), again indicating the viability of the YSZ sensor and the validity of the corrections for non-ideality (although the corrections are very small). For the more concentrated solution (1*m* Na_2SO_4), and for phosphoric acid at lower temperatures, the level of agreement is not quite so good, reflecting the lower reliability of non-ideality corrections for more concentrated solutions (in the case of 1*m* Na_2SO_4) or because

of excessive corrosion of the stainless steel cell (for phosphoric acid).

4. Applications

In this section, we describe recent applications of the YSZ sensor for measuring pH in aqueous solutions under extreme conditions of temperature, pressure, and composition. Emphasis is placed on demonstrating the versatility of the electrode for measuring pH in a wide variety of systems, many of which are of relevance to the electric power industry.

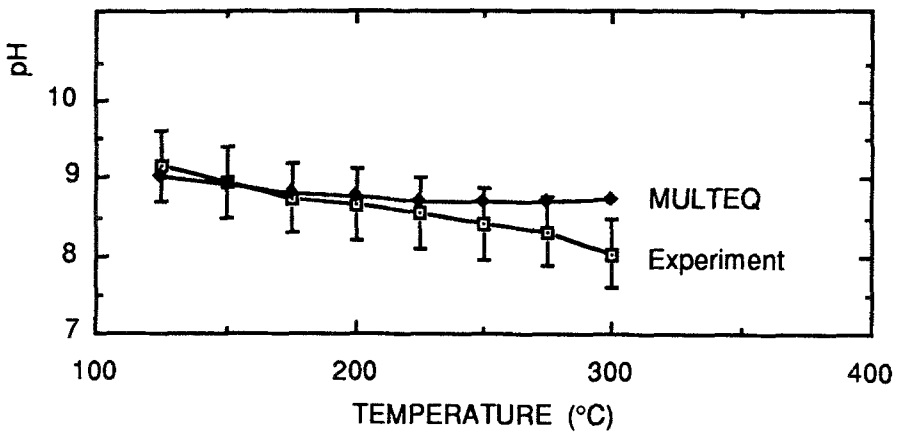

Fig. 11. Plots of pH *vs.* temperature for 1*m* NaOH + 1*m* Na_2SO_4 + 2*m* $B(OH)_3$ solution.

4.1. The $B(OH)_3/OH^-$ System

Boric acid is used in the primary circuits of pressurized water (nuclear) reactors (PWRs) as a nuclear "shim" (*i.e.*, to control reactivity), because of the high capture cross section of boron for neutrons. However, absorption of neutrons produces lithium so that, as burn up of the fuel proceeds, the pH of the primary heat transport fluid gradually increases. Because the acidity of the water can have a significant impact on corrosion and on mass and activity transport processes, a detailed understanding of the chemistry of the $B(OH)_3$/LiOH system is essential for effective control of these phenomena. Although several studies of this system under PWR primary circuit conditions at temperatures up to ~ 300°C have been reported previously, including the extensive and highly accurate work of Mesmer *et al.*,[22] measurement of the pH of various $B(OH)_3$ + MOH (M ≡ alkali metal) solutions as a function of temperature provide a good test of algorithms that have been devised to model the chemistry of the primary fluid.

One such test is shown in Fig. 10, in which pH *vs.* temperature

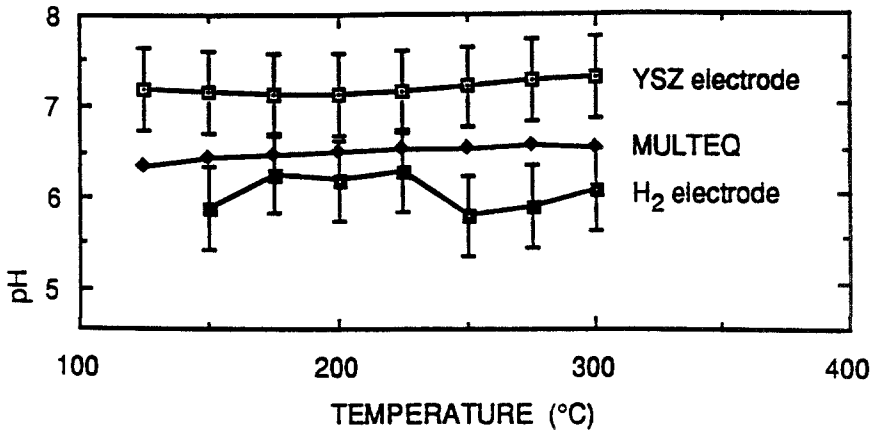

Fig. 12. Plots of pH *vs.* temperature for 1*m* NaOH + 1*m* Na_2SO_4 + 5*m* $B(OH)_3$ solution.

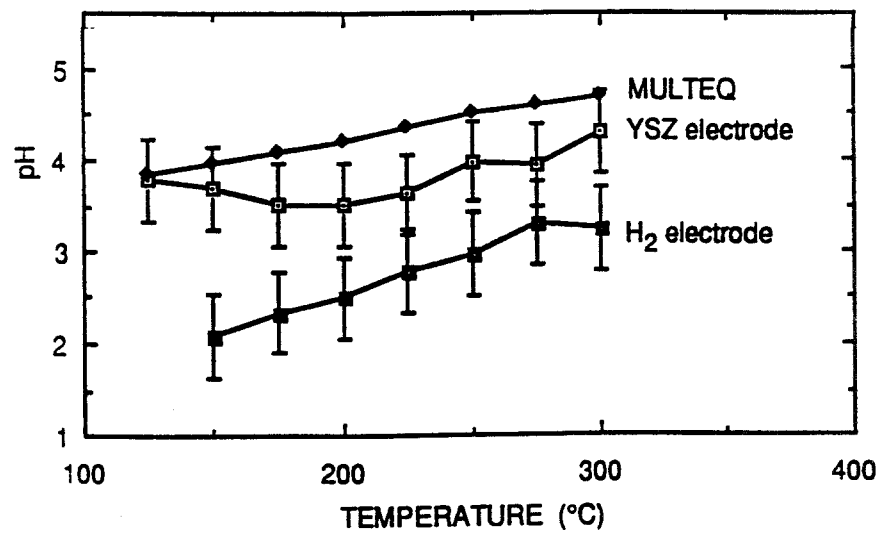

Fig. 13. Plots of pH *vs.* temperature for 1*m* NaOH + 1*m* Na_2SO_4 + 20*m* $B(OH)_3$ solution.

correlations calculated for a variety of $B(OH)_3$ + KOH solutions (KOH was chosen to avoid complications associated with ion pairing between Li^+ and OH^-) using the Electric Power Research Institute's MULTEQ code[23] are compared with experimental data. Good agreement is observed in most cases, with the two data sets seldom differing by more than 0.2 pH units.

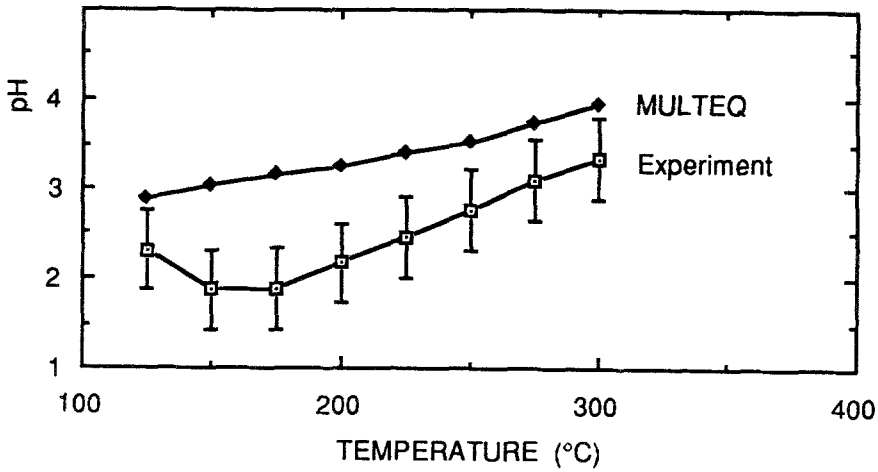

Fig. 14. Plots of pH *vs.* temperature for 1*m* NaOH + 1*m* Na_2SO_4 + 50*m* $B(OH)_3$ solution.

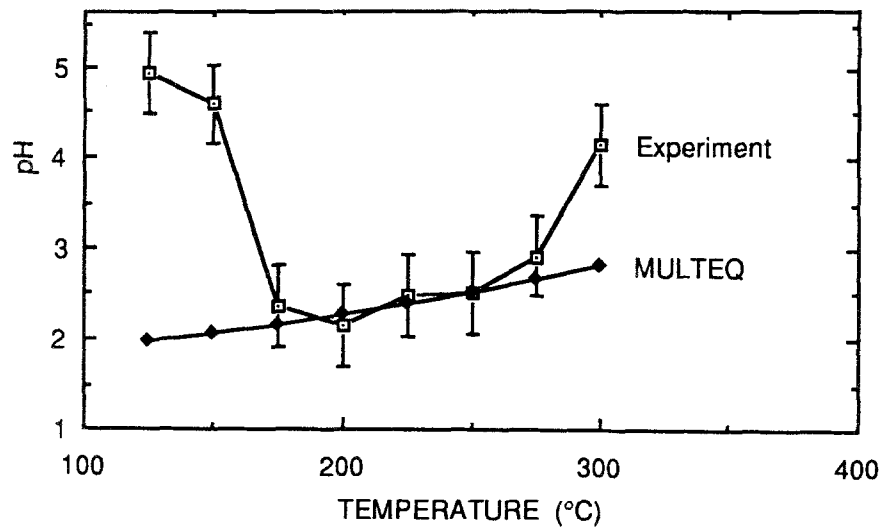

Fig. 15. Plots of pH *vs.* temperature for 1*m* NaOH + 1*m* Na_2SO_4 + 100*m* $B(OH)_3$ solution.

In a somewhat more ambitious study,[24] we measured pH *vs.* temperature correlations for a series of concentrated boric acid solutions of the type 1*m* NaOH + 1*m* Na_2SO_4 + *xm* $B(OH)_3$ with *x* ranging from 2 to 100 using both YSZ and hydrogen electrodes. Studies on this system are important from a technological viewpoint, because solutions of this

type are thought to exist in boiling crevices in the secondary sides of PWR steam generators when boric acid is added to the water to control denting corrosion. However, because of the difficulty in estimating water activities and isothermal liquid junction potentials for these solutions, and because of complications arising from glass formation at high boric acid concentrations, the measured "pH" can only be regarded as semiquantitative and as a crude indicator of the acidity of the solution. Data for solutions with $x = 2, 5, 20, 50$, and 100 are shown in Figs. 11 to 15; these data were measured using the cell shown in Fig. 16, which was equipped with a Pd/25 wt% Ag diffuser for establishing a known partial pressure of hydrogen in the environment. Also plotted are data calculated using EPRI's MULTEQ program, which incorporates activity coefficient corrections and which also provided estimates of the activity of water used in calculating the pH from the measured potential of the YSZ sensor. While the data are clearly only semiquantitative in nature, for the reasons discussed above, reasonable agreement is found between experiment and calculation, particularly at the lowest boric acid concentrations. At very high boric acid concentrations, the systems form glasses (as observed on cooling), which render both the activity of water and the isothermal liquid junction potential highly uncertain. Surprisingly, for boric acid concentrations up to 50 m, the experimental data differ from those calculated using MULTEQ by no more than one pH unit, corresponding to differences in potential of less than 120 mV. In two instances, we also plot the potential of the hydrogen electrode measured in the same system by saturating the cell with hydrogen through the Pd/25% Ag diffuser. In both cases, the pH values measured using the hydrogen electrode fall below the calculated values and the values measured with the YSZ sensor. The sources of these differences are unknown, but they might be related to the ability of the diffuser to saturate the test cell with hydrogen (in the case of the hydrogen electrode) or to a significant uncertainty in the activity of water (for the YSZ electrode). Nevertheless, the level of agreement is probably all that could be expected, given the highly non-ideal nature of the system at such high boric acid molalities. Finally, it should be noted that the pH of the most concentrated system (Fig. 15) was measured in the direction of descending temperature. Except for the highest temperature (300°C), good agreement is obtained with MULTEQ until the temperature decreases below 175°C, at which point a sharp increase in pH is observed. We attribute this increase to glass formation, which releases hydroxide ions on boric acid polymerization. From a technological viewpoint, the importance of these data is that they show that con-

centrated boric acid solutions are highly acidic but if glass formation occurs the acid is substantially neutralized. Furthermore, the data indicate that equilibrium models of the MULTEQ type may be used to estimate the pH of non-glass forming concentrated boric acid solutions to a level of accuracy that is probably sufficient for most technology purposes. In closing, it should be noted that MULTEQ incorporates the polymerization model of Mesmer *et al.*[22] to account for the formation of lower polyborates but not for the formation of glasses.

As a final example of the use of YSZ sensors to explore the $B(OH)_3$/base system, we describe below titrations of boric acid with sodium hydroxide solution. These studies were carried out as a part of our program to explore the properties of simulated crevice environments in PWR steam generators. The titrations were performed in a recirculating loop, in which aliquots of the titrant were added to the reservoir via a burette, or to a static pressure cell via a high pressure syringe pump. Typical titration curves for boric acid solutions of moderate concentrations at 25°C, obtained using a glass electrode, and at 250°C, obtained using a YSZ electrode, are shown in Figs. 17 and 18. Also plotted are titration curves calculated using a simple boric acid hydrolysis model, which ignores polyborate formation, as well as titration curves calculated using MULTEQ in which the formation of lower polyborates is taken into account. In deriving these curves, we have corrected for the changes in stoichiometric boron and sodium concentrations due to the addition of titrant to the cell. Although the level of agreement was not always as good as that displayed, these studies again confirm the ability of MULTEQ to simulate the acidity of the $B(OH)_3$/NaOH system over wide ranges of composition and temperature. Finally, the pK_b values required for the simple, non-polymer model for boric acid to simulate the measured data are in reasonable agreement with literature values.

4.2. Simulation of PWR Secondary Environments

In addition to the studies on the $B(OH)_3$/base systems reported above, we have also measured pH *vs.* temperature correlations for a variety of solutions that are thought to model crevice environments on the secondary side of a PWR steam generator (Figs. 19 and 20). These solutions contain solutes that enter the steam generator as impurities in the feedwater (silicates, organic acids, and inorganic ions such as Ca^{2+} and SO_4^{2-}), as corrosion products from the condensers (*e.g.*, $CuCl_2$ for plants containing copper alloys) or as water treatment chemicals (*e.g.*, phosphates). We also plot pH *vs.* temperature correlations for concentrated natural cooling waters (*e.g.*, "Mississippi River Water" and

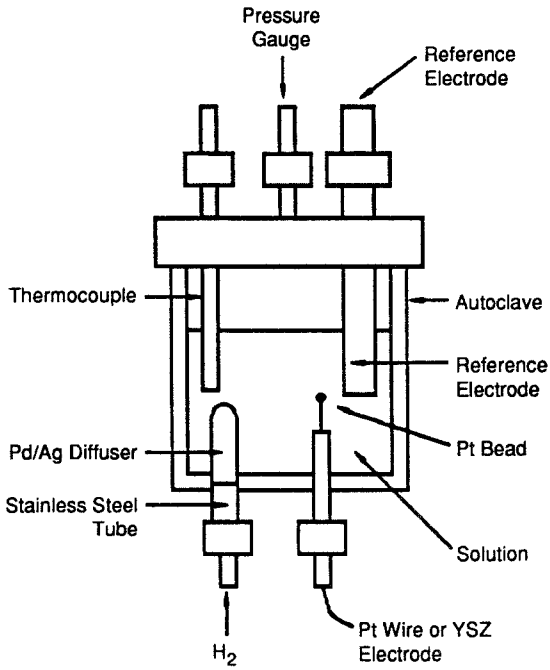

Fig. 16. Schematic of static test cell showing electrode configuration for measuring the pH of concentrated solutions at elevated temperatures.

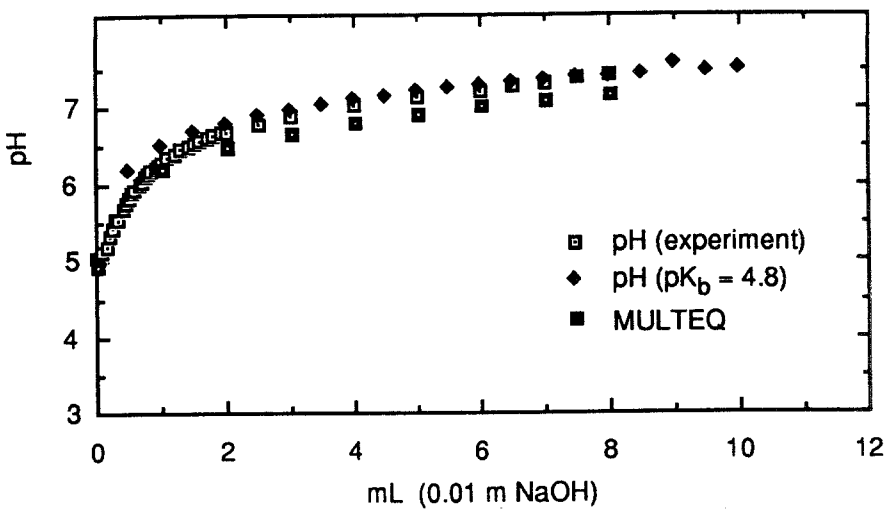

Fig. 17. Titration of 50 mL of 0.1*m* boric acid with 0.01*m* at NaOH at 25°C (conventional pH meter). The experimental data are compared with theoretically calculated values assuming $pK_b = 4.8$.

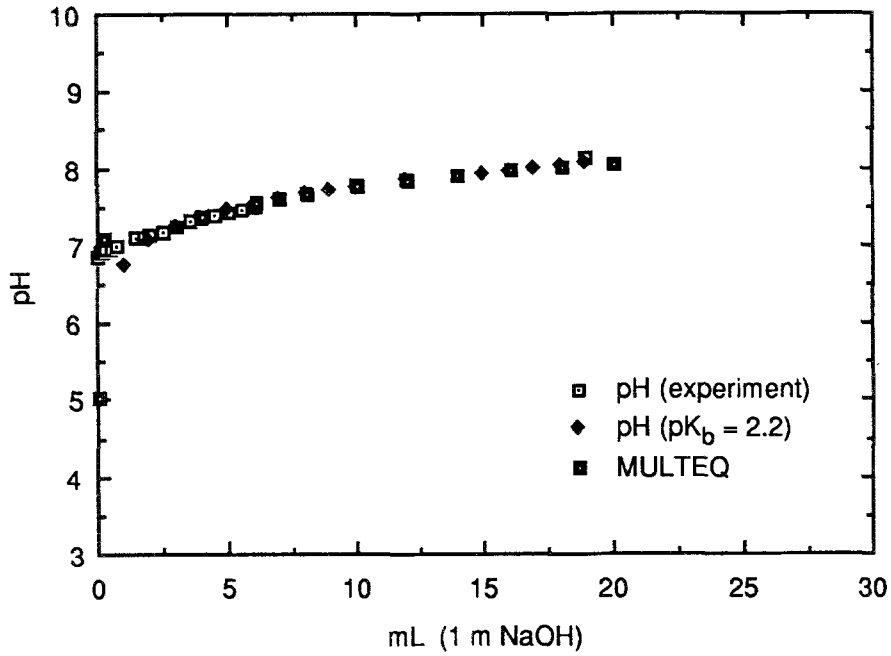

Fig. 18. Titration of 1950 mL of 0.1*m* boric acid with 1*m* at NaOH at 250°C (circulation type titration). The experimental data are compared with theoretically calculated values assuming $pK_b = 2.2$.

"Lake Michigan Water," as calculated using MULTEQ), to simulate in-leakage through faulty condensers. In all cases, the solute concentrations are much higher than found in the bulk water; the higher concentrations are used to simulate environments that are thought to exist at boiling surfaces, in crevices, and possibly in "sludge" piles on the support plates and tubesheet. It is clear from these measurements that the simulated environments differ widely in their acid/base properties, suggesting that environments of equally variable pH may exist in operating steam generators. Of particular interest are the low pH values displayed by 0.1*m* $CuCl_2$, because copper has been implicated in "denting" corrosion that occurs in the crevices between the Alloy 600 tubes and carbon steel support plates in the steam generators of PWRs equipped with copper alloy condensers or feedwater heaters.[25] However, previous studies[26] have shown that it is not the acidity *per se* that is responsible for the fast growth of magnetite on carbon steel, but the presence of easily reduced cations (*e.g.*, Cu^{2+}) that effectively depolarize the cathode of the corrosion couple and/or provide a catalytic surface for

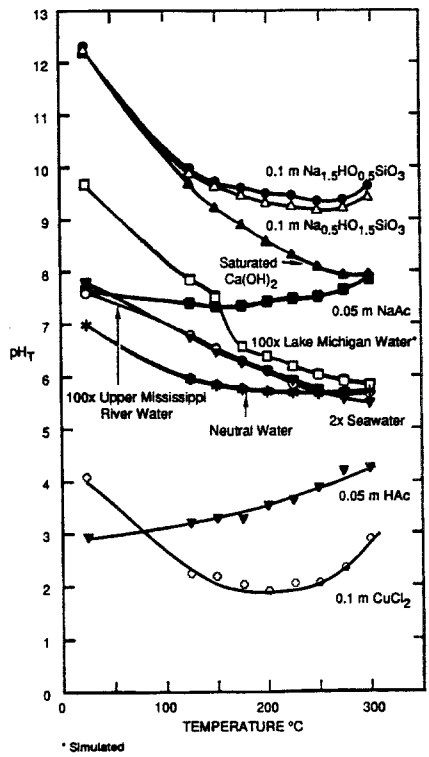

Fig. 19. Dependence of pH of simulated crevice solutions on temperature.

hydrogen evolution. Copper has also been implicated in pitting and possibly intergranular attack on Alloy 600 steam generator tubes; in these cases, the low pH due to hydrolysis of Cu^{2+} (Fig. 19) as well as the ability of Cu(II) to displace the corrosion potential in the positive direction, coupled with a susceptible microstructure, are probably the most important factors in causing damage to the tubes.

4.3. Salt Repositories for High Level Nuclear Waste

Geologically-stable salt domes are currently being considered as repositories for the permanent disposal of high level nuclear waste (HLNW). The concept calls for the disposal of canisters containing the wasteform in caverns mined from the salt; the caverns are ultimately back-filled with crushed salt, and creep of the surrounding matrix will eventually result in the canisters being encapsulated in rock salt. Because the canisters emit heat from radioactive decay and because the solubility of salt increases with temperature, brine inclusions contained

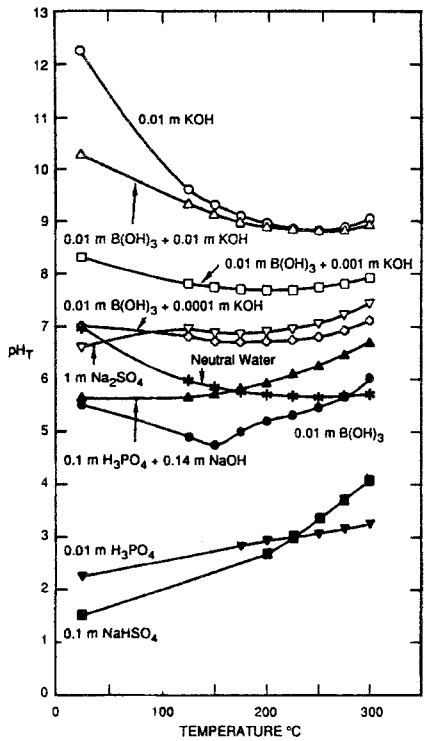

Fig. 20. Dependence of pH of standard solutions on temperature.

within the salt will move up the temperature gradient towards the canisters. Indeed, depending on the type of waste and the design of the canisters and the repository, the temperature at the surface of a canister may be as high as 250°C soon after closure of the repository, with an ultimate decay to ambient at a half-life as long as several hundred years. Accordingly, we expect that eventually the canisters will become bathed in saturated brine at the canister surface temperature. Furthermore, the brine is subject to γ-radiolysis, albeit at moderate does rates ($\sim 2\times10^5$ rad-h^{-1}), which is expected to yield, on balance, an oxidizing environment. Because geological brines frequently contain significant amounts of Mg^{2+}, hydrolysis is expected to produce an acidic environment which, together with the oxidizing conditions produced by radiolysis, could pose a threat to the integrity of the canister depending on the material of fabrication. To explore this issue, we have used the YSZ sensor to measure pH/concentration/temperature surfaces for the NaCl-$MgCl_2$-H_2O system across the entire composition range and at temperatures

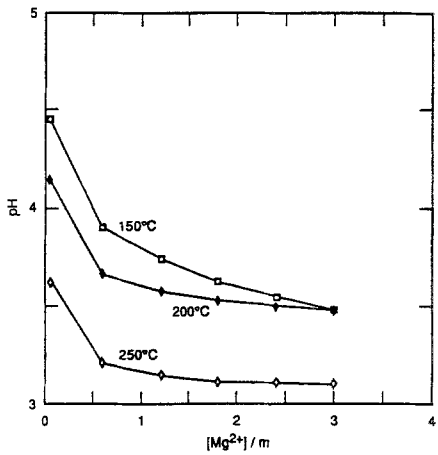

Fig. 21. Variation of pH with $[Mg^{2+}]$ for $MgCl_2^-$ (1.8*m*) NaCl-H_2O solutions as a function of temperature.

from 125 to 250°C.[27]

Examples of the data measured in this study, which will be analyzed in depth elsewhere,[27] are shown in Fig. 21. These data indicate that for a temperature of 250°C, and at high Mg^{2+} concentrations, the pH could be as low as 3.0. We believe that acidities of this magnitude, coupled with the oxidizing redox environment generated by γ-radiolysis, do indeed pose a serious threat to the long term integrity of canisters fabricated from most common metals and alloys (*e.g.*, carbon steel and copper alloys). To our knowledge, the data reported here are the first to have been measured on saturated brines under conditions relevant to the disposal of high level nuclear waste in salt repositories.

4.4. Supercritical Aqueous Systems

The physico-chemical properties of aqueous systems at supercritical temperatures (T > 374°C for pure water) are of great theoretical and practical interest, because of the unusual phenomena that occur on transitioning the critical temperature (*e.g.*, the compressibility at T_c is infinite and the density of the fluid is an independent variable at $T > T_c$), and because supercritical aqueous systems are involved in processes ranging from power generation (in supercritical fossil units) to mineralization in geochemical systems. While considerable work has been reported on measuring the PVT properties and electrical conductivities of such systems, no studies have been reported on measuring the

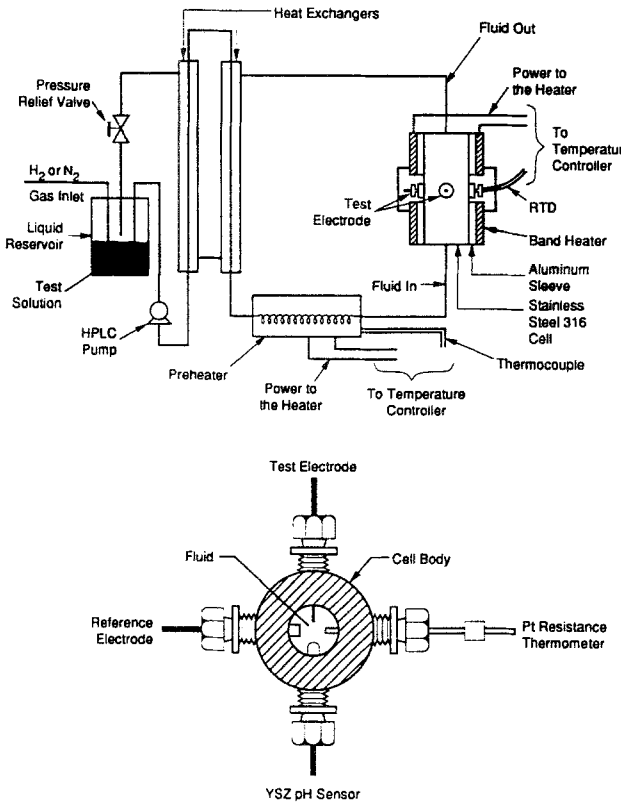

Fig. 22. Schematic of the loop and a cross sectional view of the cell used for pH studies in aqueous solutions at supercritical temperatures.

pH. However, we recently extended our pH measuring capabilities using YSZ electrodes to supercritical temperatures by developing an EPBRE that can operate for short periods of time at temperatures above 400°C. Details of these studies will be published elsewhere. In this paper, we report the results of some of this work in general form, with the purpose of demonstrating the current state-of-the-art in measuring pH at supercritical temperatures.

The apparatus used in our studies is shown schematically in Fig. 22. Briefly, the cylindrical Hastelloy-C test cell was contained in a once-through Hastelloy-C recirculation flow system activated by a HPLC (High Pressure Liquid Chromatography) pump. The desired chemistry conditions in the fluid could be established by sparging the reservoir with hydrogen at ambient temperature. The cell contained ports for a YSZ pH sensor, a reference electrode, a Pt hydrogen

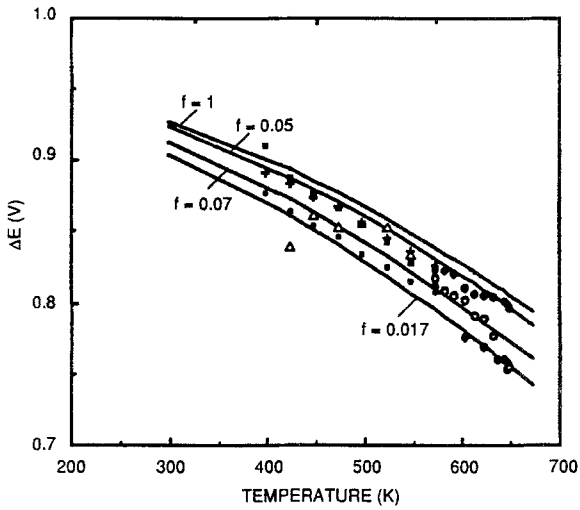

Fig. 23. Potential (ΔE) of the cell $H_2/H^+/ZrO_2(Y_2O_3)/HgO/Hg$ as a function of temperature for various test solutions and hydrogen fugacities f. ♦, 0.0001m HCl; ♦, 0.001m HCl; o, 0.001m NaOH; ▲, 0.01m H_3PO_4; •, 1m $NaSO_4$; +, 0.01m $B(OH)_3$ + 0.01m KOH; and ■, 0.01m KOH.

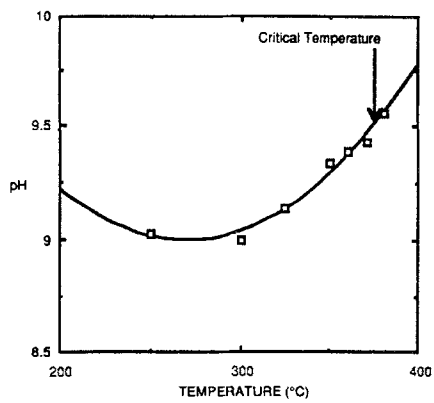

Fig. 24. Variation of pH as a function of temperature for 0.01m KOH.

electrode, and a Pt-resistance thermometer. The cell could be operated at temperatures in excess of 400°C and at pressures up to 300 bar.

To test the thermodynamic viability of the YSZ electrode at temperatures into the supercritical region, we plot data in Fig. 23 for the cell $H_2/H^+/ZrO_2(Y_2O_3)/HgO/Hg$ as a function of temperature. Also plotted

are theoretical correlations of ΔE *vs.* T, as calculated using Eq. (19), for hydrogen partial pressures ranging from 0.017 to 1.0 atm. These correlations were calculated to account for the scatter in the experimental data, which we attribute to variations in the fugacity of hydrogen in the test cell due to losses through the walls of the apparatus. While the data are only semiquantitative in quality, we did not detect any discontinuity in the cell voltage as the temperature transitioned the critical temperature. This was expected since the cell voltage is given by the zeroeth derivative of the change in Gibb's energy.

Because the EPBRE used in this work had been calibrated to the SHE scale, the potential of the YSZ electrode measured with respect to this reference could be used to calculate the pH of the solution. A plot of pH *vs.* temperature for 0.01*m* KOH from 200°C to 380°C is shown in Fig. 24. The highest temperature is greater than T_c for pure water (374°C) and is estimated to be just above the critical temperature of ~375°C calculated for 0.01*m* KOH according to the data of Marshall.[28] Again, the curve transitions the critical region continuously. Note that, in calculating the pH, we used extrapolated values for the activity of water estimated from the MULTEQ computer code. To our knowledge, the data plotted in Fig. 24 represents the first attempt to extend pH measurements to temperatures above the critical temperature of water.

5. Summary and Conclusions

In this paper, we review the use of yttria-stabilized zirconia (YSZ) electrodes of the type $Hg/HgO/ZrO_2(Y_2O_3)/H^+$ for measuring pH in aqueous solutions at high subcritical ($150 < T_c < 374°C$) and supercritical ($T > 374°C$) temperatures. We discuss the construction and operation of YSZ and reference electrodes used in our laboratory for these measurements, and we illustrate their use with reference to studies on boric acid/base buffer solutions (including highly concentrated systems), simulated pressurized water reactor (PWR) secondary-side steam generator crevice environments, and on $NaCl\text{-}MgCl_2\text{-}H_2O$ systems simulating brine inclusions in rock salt high level nuclear waste repositories. Finally, we describe recent work extending pH measurements to temperatures above the critical temperature of water. Our studies have shown that:

1. The YSZ pH sensor is thermodynamically viable, in that it responds correctly to changes in pH when compared with a hydrogen electrode in the same solution. Because the

potential of the sensor can be calculated thermodynamically, the YSZ electrode is a primary pH sensor;

2. The principal obstacle to highly accurate pH measurements at temperatures into the supercritical range is the lack of an accurate reference electrode;

3. Using existing reference electrodes, particularly the EPBRE, technologically useful pH measurements can be made on a wide variety of aqueous systems at temperatures ranging from 150°C to greater than 374°C; and

4. The further development of YSZ electrodes as accurate pH sensors for high subcritical and supercritical aqueous systems will require precise knowledge of the activity of water and the isothermal liquid junction potential over wide ranges of composition and temperature.

Finally, the work outlined in this paper demonstrates that the Electric Power Research Institute's MULTEQ chemistry program is effective for estimating pH *vs.* temperature correlations for a wide variety of aqueous systems of importance to the electric power generating industry.

Acknowledgment

The authors gratefully acknowledge support of this work by the Electric Power Research Institute, Palo Alto, California, through a number of contracts over the past ten years and by SRI International through the Internal Research and Development (IR&D) program.

References

1. R. G. Bates, *Determination of pH, Theory and Practice* (Wiley-Interscience, New York, 1973).
2. R. E. Mesmer, *Geochim. et Cosmochim. Acta* **55**, 1171 (1991).
3. D. D. Macdonald, S. Hettiarchchi, and S. J. Lenhart, *J. Solution Chem.* **17**, 719 (1988).
4. L. W. Niedrach, *J. Electrochem. Soc.* **127**, 2122 (1980).
5. T. Tsuruta and D. D. Macdonald, *J. Electrochem. Soc.* **129**, 1221 (1982).
6. S. Hettiarachchi and D. D. Macdonald, *J. Electrochem. Soc.* **131**, 2206 (1984).
7. S. Hettiarachchi, P. Kedzierzawski, and D. D. Macdonald, *J. Electrochem. Soc.* **132**, 1866 (1985).

8. M. J. Danielson and O. H. Koski, *J. Electrochem. Soc.* **132**, 296 (1985); **132**, 2037 (1985).
9. C-T. Liu and W. T. Lindsay, *J. Solution Chem.* **1**, 45 (1972).
10. D. J. G. Ives and G. J. Janz, *Reference Electrodes* (Academic Press, New York, 1961).
11. D. D. Macdonald, *Corrosion* **34**, 75 (1978).
12. D. D. Macdonald, A. C. Scott, and P. R. Wentrcek, *J. Electrochem. Soc.* **126**, 908 (1979).
13. K. Makela, S. Hettiarachchi, R. Emerson, and D. D. Macdonald, unpublished data.
14. W. Bogaerts and A. A. Van Haute, *Proc. Int. Congr. Met. Corros.* **4**, 169 (1984) [published by Nat. Res. Council Canada].
15. D. D. Macdonald, A. C. Scott, and P. R. Wentrcek, *J. Electrochem. Soc.* **126**, 1618, (1979).
16. P. Henderson, *Z. Physik. Chem.* **59**, 118 (1907); **63**, 325 (1908).
17. C. F. Baes and R. E. Mesmer, *Hydrolysis of Cations* (Wiley-Interscience, New York, 1976).
18. J. Pang and D. D. Macdonald, to be published.
19. R. S. Greeley, W. T. Smith, R. W. Stoughton, and M. H. Lietzke, *J. Phys. Chem.* **64**, 652, 1445, 1861 (1960).
20. D. D. Macdonald, in *Modern Aspects of Electrochemistry*, Vol. 11, B. E. Conway and J. O'M. Bockris, eds., (Plenum Press, New York, (1975) p. 141.
21. G. B. Naumov, B. N. Ryzhenko, and I. L. Khodakovsky, *Handbook of Thermodynamic Data*, USGS-WRD-74-001 (1974).
22. R. E. Mesmer, C. F. Baes, and F. H. Sweeton, *Inorg. Chem.* **11**, 537 (1972).
23. J. P. Paine and P. Millett, private communications.
24. H. Song, D. D. Macdonald, C. Shoemaker, and J. P. Paine, in *Proc. Fourth Int. Symp. Environ. Degrad. Mat. Nucl. Power Systs. - Water Reactors*, D. Cubicciotti, ed., (NACE, Texas, 1990), p. 12.
25. R. Garnsey, *Nucl. Energy* **18**, 2 (1979).
26. J. R. Park and D. D. Macdonald, *Corrosion* **45**, 563 (1988).
27. M. Ben-Haim and D. D. Macdonald, to be published (1991).
28. W. L. Marshall and E. V. Jones, *J. Inorg. Nucl. Chem.* **36**, 2313 (1974).